Using Magnetic Droplet Nucleation to Determine the Spin Torque Efficiency and Asymmetry in $Co_x(Ni,Fe)_{1-x}$ Thin Films

Sheng Jiang,[1,2] Sunjae Chung,[1,3,*] Quang Tuan Le,[1,4] Hamid Mazraati,[1,2] Afshin Houshang,[2,4] and Johan Åkerman[1,2,4,†]

[1] *Department of Applied Physics, School of Engineering Sciences, KTH Royal Institute of Technology, Electrum 229, SE-16440 Kista, Sweden*
[2] *NanOsc AB, Kista 164 40, Sweden*
[3] *Department of Physics and Astronomy, Uppsala University, 751 20 Uppsala, Sweden*
[4] *Department of Physics, University of Gothenburg, 412 96, Gothenburg, Sweden*

We demonstrate how to extract the material-dependent spin-torque efficiency (ϵ) and asymmetry (λ) from the field-current nucleation boundaries of magnetic droplet solitons in orthogonal nano-contact spin-torque oscillators with $Co_x(Ni_{80}Fe_{20})_{1-x}$, ($x = 0 - 1$), fixed layers. As the perpendicular component of the fixed-layer magnetization plays a central role in governing droplet nucleation, the nucleation boundaries exhibit monotonic shifts towards higher perpendicular magnetic fields when the fixed-layer magnetization $\mu_0 M_{s,p}$ is tuned from 1.04 to 1.7 T. We then extract ϵ and λ from fits to the nucleation boundaries and find that while ϵ does not vary with composition, λ increases from 1.5 to 3 with increasing Co content. The analysis of droplet nucleation boundaries is hence a useful tool for the systematic study of both ϵ and λ as functions of material composition.

I. INTRODUCTION

Magnetic droplets are characterized as dynamic, non-topological magnetic solitons. They occur in magnetic thin films with perpendicular magnetic anisotropy (PMA), and exhibit a reversed core with a precessing boundary [1,2]. Magnetic droplets were first described 40 years ago in an ideal zero-damping medium [3], and their possible realization was later predicted theoretically [1] using spin-torque nano-oscillators (STNOs) [4] with PMA free layers [5,6]. The first experimental demonstration of magnetic droplets was reported in STNOs with a PMA [Co/Ni] free layer and a Co fixed layer [2]. The droplet has attracted much attention due to its interesting characteristics, such as a highly nonlinear dynamics [7–9], large power emission [2], and possible applications in microwave-assisted magnetic recording (MAMR) [10,11]. Several theoretical [8,12–17] and experimental [18–28] studies on magnetic droplets have since been presented.

Recently, the details of the droplet nucleation boundary has attracted particular interest [25,26,29]. As explained in [25], it can be very well described using a simple form of the equation that considers the current-field phase diagram [25]:

$$I_n = \alpha A H + B/H + C, \tag{1}$$

where I_n and H are the nucleation current and applied magnetic field, respectively. α is the damping of the free layer. The coefficients A, B, and C are associated with the magnetic properties of the fixed and free layers, such as the fixed-layer saturation magnetization $\mu_0 M_{s,p}$ and magnetic anisotropy field $\mu_0 H_{k,p}$ [25]. Equation (1) also holds when the current-induced Oersted field is taken into account [29]. It therefore offers the possibility to tailor the droplet nucleation boundary by varying the fixed-layer magnetic properties, so as to further optimize the device design for practical spintronic applications.

In this paper, we demonstrate such control of the droplet nucleation boundary by tailoring one of the major parameters—$\mu_0 M_{s,p}$ of the $Co_x(Ni_{80}Fe_{20})_{1-x}$ fixed layers—while maintaining the same PMA [Co/Ni] free layer. The droplet nucleation boundaries are determined for five different compositions ($x = 0, 0.25, 0.5, 0.75,$ and 1) and four different NC sizes ($R_{NC} = 35, 40, 45,$ and 50 nm). As expected from the model, the nucleation boundary moves to higher fields as $\mu_0 M_{s,p}$ of the $Co_x(Ni_{80}Fe_{20})_{1-x}$ fixed layer increases from 1.04 to 1.7 T with increasing Co content. We then extract the spin-torque efficiency (ϵ) and the spin-torque asymmetry (λ) from fits of Eq. (1) to the nucleation boundaries. We find a largely composition-independent spin-torque efficiency of $\epsilon = 0.3$–0.4, in good agreement with literature values [30]. In contrast, the extracted spin-torque asymmetry increases from 1.5 for NiFe to 3 with Co. Our results hence demonstrate how the

---
*mcskj1976@gmail.com
†akerman1@kth.se

analysis of droplet nucleation boundaries can be a useful tool for the systematic study of ϵ and λ as functions of material composition, and that λ of $Co_x(Ni_{80}Fe_{20})_{1-x}$ thin films can be tuned by varying the Co content.

II. EXPERIMENTAL DETAILS

The orthogonal spin-valve stacks, consisting of a Ta(4)/Cu(12)/Ta(4) seed layer, a $Co_x(Ni_{80}Fe_{20})_{1-x}(6)$/Cu (7)/[Co(0.25)/Ni(0.6)] × 4/Co(0.25) spin valve, and a Cu(2)/Pd(2) capping layer, are deposited on thermally oxidized Si wafers using magnetron sputtering (the numbers in parentheses are layer thicknesses in nanometers). The different compositions of the fixed layer are controlled by varying the respective deposition rates during cosputtering of the $Ni_{80}Fe_{20}$ and Co targets. The spin-valve structure is magnetically orthogonal: the fixed layer has an easy-plane magnetic anisotropy, while the free layer, [Co/Ni] × 4/Co, has strong PMA. The stacks are then patterned into 8 × 16 μm^2 mesas by means of optical lithography and ion-milling etching, followed by CVD of a 30-nm-thick insulating SiO_2 film. Electron-beam lithography and reactive ion etching are used to open nano-contacts with nominal radii R_{NC} varying from 35 to 50 nm, through SiO_2 in the center of each mesa. The fabrication is completed by deposition and lift-off lithography of a Cu(500 nm)/Au(100 nm) top electrode. A schematic view of the STNO is shown in Fig. 1(a).

Broadband ferromagnetic resonance (FMR) is measured using a NanOsc Instruments PhaseFMR spectrometer to extract the saturation magnetization $\mu_0 M_{s,p}$ of the $Co_x(Ni_{80}Fe_{20})_{1-x}$ films from magnetic-field sweeps in the $\mu_0 H = 0$ to 0.35 T field range. For dc and microwave characterization, we use our custom-built probe station, capable of independently controlling the direct current, the magnetic-field magnitude (up to 2 T), and the field direction. In the present experiment, the field is applied normal to the film plane. The direct current is injected into the device using a Keithley 6221 current source, and the dc voltage is measured with a Keithley 2182 nanovoltmeter. The sign of the applied direct current is negative, meaning the electrons flowed from the free to the fixed layer in order to obtain spin-transfer-torque- (STT-)induced magnetization dynamics [31–34] in the free layer. The generated microwave signals are decoupled from the dc voltage via a bias tee and are amplified using a low-noise amplifier prior to being recorded by a spectrum analyzer (R&S FSU 20 Hz–67 GHz).

III. RESULTS AND DISCUSSION

Figure 1(b) shows the $Co_x(Ni_{80}Fe_{20})_{1-x}$ resonance fields H_{res} extracted from FMR measurements at different constant rf frequencies. The measurements are shown as solid dots while the solid lines are fits to Kittel's
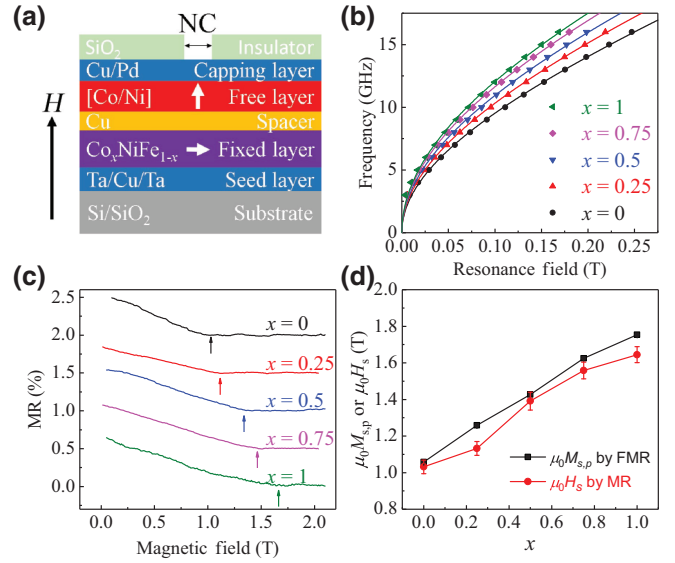

FIG. 1. (a) Schematic of a spin-torque nano-oscillator (STNO) device. The nominal radius of nano-contact (NC) R_{NC} is between 35 and 50 nm. (b) Ferromagnetic resonance field $\mu_0 H_{res}$ vs. frequency measured for different $Co_x(Ni_{80}Fe_{20})_{1-x}$ compositions. (c) MR vs. applied perpendicular field (shifts added to distinguish between curves; arrows indicate saturation fields). (d) Saturation magnetization $\mu_0 M_{s,p}$, obtained by fitting the Kittel equation to H_{res}, and saturation fields $\mu_0 H_s$, determined by MR of the STNOs as a function of x.

equation [35],

$$f = \frac{\gamma \mu_0}{2\pi}\sqrt{H_{res}(H_{res} + M_{eff})}, \quad (2)$$

where f is the microwave frequency, $\gamma/2\pi$ is the gyromagnetic ratio, μ_0 is the permeability of free space, and M_{eff} is the effective magnetization, here assumed identical to $M_{s,p}$, since the in-plane magnetic anisotropy H_k of $Co_x(Ni_{80}Fe_{20})_{1-x}$ films is negligible.

From magnetoresistance measurements at low current ($I = -1$ mA) under a magnetic field $\mu_0 H$ perpendicular to the film plane, the field-dependent resistance changes. MR = $[R(H) - R_P]/R_P$ [R_P is the device resistance in the magnetically parallel state of both Co/Ni and $Co_x(Ni_{80}Fe_{20})_{1-x}$ layers], [18,22] is determined as shown in Fig. 1(c). $\mu_0 M_{s,p}$ tilts gradually under the influence of the increasing perpendicular magnetic field and finally saturates along the field direction. Consequently, MR gradually decreases to R_P at the saturation field, $\mu_0 H_s$, where both the fixed and free layers align with the direction of the magnetic field. $\mu_0 H_s$ for each $Co_x(Ni_{80}Fe_{20})_{1-x}$ fixed layer is indicated by an arrow in Fig. 1(c). Figure 1(d) shows how the fixed-layer saturation magnetization ($\mu_0 M_{s,p}$) and its out-of-plane saturation field ($\mu_0 H_s$) are linearly increasing with x. The slightly lower $\mu_0 H_s$ from MR measurement compared to $\mu_0 M_{s,p}$ from FMR measurement is likely due to some process-induced changes in the final devices.
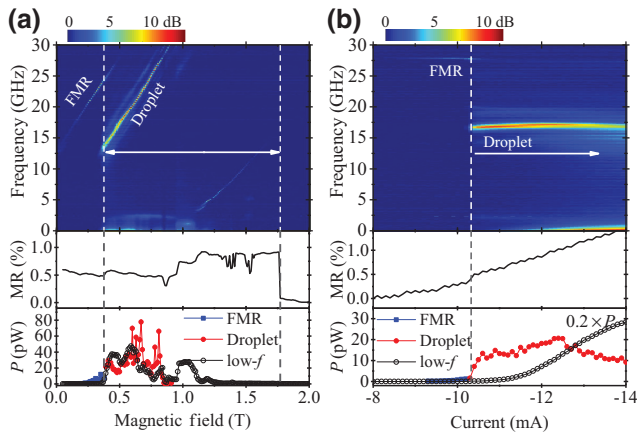
FIG. 2. Frequency f, MR, and integrated power P as functions of (a) perpendicular field at $I = -12$ mA and (b) direct current at $\mu_0 H = 0.5$ T for a $R_{NC} = 40$ nm STNO with $x = 0.5$. FMR and Droplet refer to the FMR-like mode and droplet mode, respectively. Droplet nucleation is detected as a jump in MR, a drop in the microwave frequency, an increase in the integrated power, and the appearance of low-frequency (< 2 GHz) microwave noise. The vertical dotted lines and arrows indicate nucleation boundaries of the magnetic droplet for the given conditions.

Microwave and dc measurements are carried out to determine the magnetic droplet nucleation and annihilation points. Figure 2 presents some typical results obtained from a device with a nominal NC radius of 40 nm and $x = 0.5$. In Fig. 2(a), where a constant $I = -12$ mA is applied, moderate microwave signals appear as the field increases, as expected from the current-induced FMR-like precession in STNOs. At $\mu_0 H = 0.38$ T, however, an abrupt frequency drop of about 10 GHz occurs, accompanied by an increase in the integrated emission power P of more than one order of magnitude. The onset of low-frequency noise (< 2 GHz), is the consequence of the drift instability of the droplet [22,25]. All of these observations point to the nucleation of a magnetic droplet at $\mu_0 H = 0.38$ T. The droplet is then sustained up to a field of 1.77 T, where MR drops to zero and the droplet is thus annihilated. The faint microwave signals in the high-field region (1.14 to 1.60 T) may be related to oscillatory motion [2] or parametric modulation of the droplet perimeter [14]. Current-sweep measurements at a fixed field of $\mu_0 H = 0.5$ T [see Fig. 2(b)] show similar characteristics of the droplet nucleation seen at $I = -10.3$ mA. In brief, all these experimental observations—MR jump, microwave frequency drop, and appearance of the low-frequency noise—are used to trace the nucleation and annihilation of magnetic droplets, as described in previous works [2,18,22,25,26].

By conducting detailed field-sweep and current-sweep measurements, as shown in Fig. 2, we determine the entire nucleation boundaries in all devices with different NC radii and fixed-layer compositions. The results are shown

as solid symbols presented in Figs. 3(a)–3(e). All of the nucleation boundaries show a similar behavior: the nucleation current I_n first decreases almost inversely with H in the low-field regime, and then start to increase with H in the high-field regime. These contrasting tendencies result from two different types of underlying physics, related to the device characteristics and the theory of magnetic droplets [1,2,18,22,25,26]. On the one hand, the perpendicular component of the fixed-layer magnetization, M_z, increases with increasing magnetic field along the z direction, which, in turn, leads to a proportional increase in the magnitude of the spin-transfer torque [2,25] and consequently lowers the current required to nucleate a droplet, i.e., $I_n \propto 1/H$. On the other hand, increasing the magnetic field H raises a critical current condition for the onset of instability to drive the magnetic droplet from its uniformly magnetized state. Slonczewski's critical current condition [33,34], which involves PMA with weak perturbations, clearly demonstrates a linear dependency ($I_n \propto H$) in this case. The observed boundaries are dictated by both contributions to different degrees.

To quantitatively study the droplet nucleation boundary, the experimental data described above is fitted with Eq. (1), as suggested in Ref. [25]. Equation (1) indeed consists of a linear ($\alpha A H$) and an inverse (B/H) term. While it is worthwhile noting that (i) this analytical Eq. (1) is only valid up to saturation of $\mu_0 M_{s,p}$ in the fixed layer, based on the theory developed in Ref. [25], (ii) this analytical model did not consider any impact of the Oersted field on the magnetodynamics of STNOs, though Oersted fields have a critical role to explain many experimental observations [36–41]. The impact of the Oersted field on nucleation boundary has been recently studied and Eq. (1) has been improved and can in practice be extended to larger magnetic field than $\mu_0 M_{s,p}$, as described in Ref. [29]. All experimental results here are fitted with this modified fitting equation [29],

$$I_n = \alpha A H + \frac{B}{M_{s,p} \cos\theta} + C, \quad (3)$$

where θ is the angle between fixed-layer magnetization direction to film normal. The solid lines in Figs. 3(a)–3(e) show the fitted results; all fits are in good agreement with the experimental data. The nucleation boundary of some devices, e.g., the device with $R_{NC} = 50$ nm and $x = 0.75$ in the field range 0.4 and 1.0 T [Fig. 3(d)], show deviations from the fits, most often around the current minimum. These deviations likely originate from a substantial drift instability [22,25,42], and seem to affect different devices to a varying degree.

The fitted coefficients in Eq. (1), αA and B, are then extracted and plotted in Figs. 3(f)–3(j) as functions of the nominal NC area (πR_{NC}^2) for different values of x. The linear dependency on NC area of both parameters [solid lines shown in Figs. 3(f)–3(j)] is consistent with the
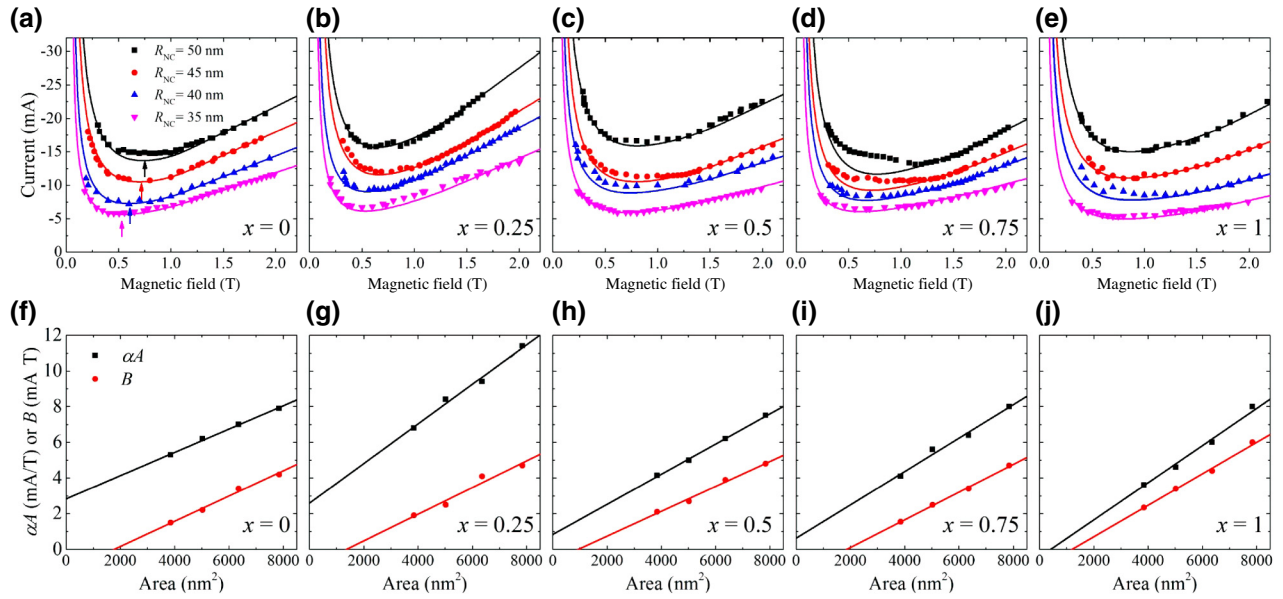
FIG. 3. (a)–(e) *I–H* maps of magnetic droplet nucleation boundaries for five different fixed-layer compositions and four different NC radii, with fits including the Oersted field effects. The arrows in (a) indicate the minimal fields H_{min}. (f)–(j) Extracted coefficients αA and B as functions of nano-contact area, πR_{NC}^2, for different x. Solid lines are linear fits.

analytical model. It can be seen that there are some disagreements regarding the interceptions of both αA and B in the limit $R_{NC}^2 \to 0$. We argue that this disagreement results from neglecting higher orders of expansion in solving the LLGS equations [25]. Furthermore, device-to-device variations and the thermal excitation of magnons could also contribute to this discrepancy.

Each nucleation boundary shows a minimum point (H_{min}, I_{min}), which can be extracted from the fits. These results are presented in Fig. 4(a) for different values of x to illustrate the ability of nucleation boundary engineering. As x ($M_{s,p}$) increases, $\mu_0 H_{min}$ also increases monotonically, with some fluctuation, possibly originating from the magnetic properties of the fixed layer, such as the exchange length l_{ex}, as well as from physical defects in the devices. This means that the nucleation boundary shifts towards higher fields as $\mu_0 M_{s,p}$ of the fixed layer increases. Meanwhile, I_{min} fluctuates more strongly from device to device and thus is not shown.

We finally turn to the main result of our study—the simultaneous extraction of both the spin-torque efficiency ϵ and the spin-torque asymmetry λ as a function of the $Co_x(Ni_{80}Fe_{20})_{1-x}$ fixed-layer composition. As mentioned in Eqs. (24)–(25) of Ref. [25], αA and B are linearly proportional to the NC area, with their respective slopes, $S_{\alpha A}$ and S_B, as below:

$$S_{\alpha A} = \frac{\alpha \nu j_0}{\pi M_s}, \tag{4}$$

$$S_B = \frac{\alpha j_0 M_{s,p}}{\pi}\left(\frac{H_{k,p}}{M_s} - 1\right), \tag{5}$$

where $j_0 = (\lambda^2 + 1)M_s^2 e\mu_0\pi\delta/(\hbar\epsilon\lambda^2)$ is the scaling current density, $\nu = (\lambda^2 - 1)/(\lambda^2 + 1)$ is the normalized asymmetry coefficient, e is the electron charge, $\alpha = 0.03$, and M_s is the saturation magnetization of the free layer.
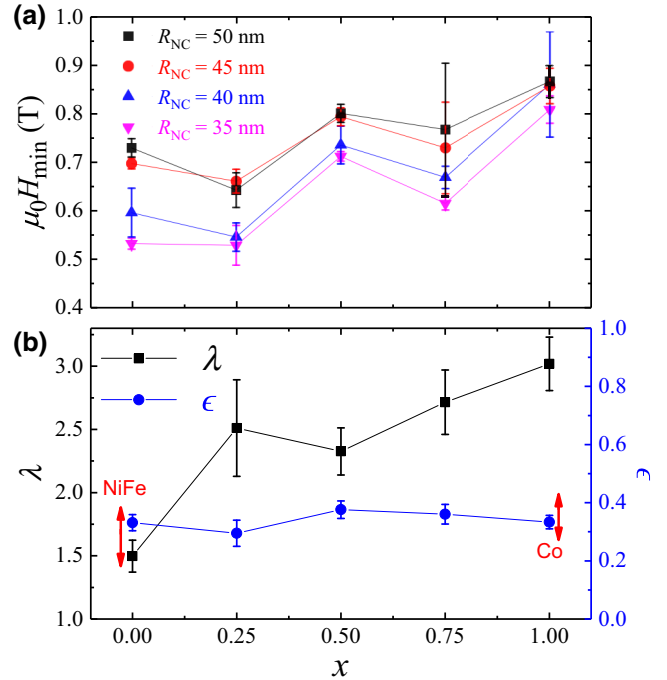

FIG. 4. (a) $\mu_0 H_{min}$ as a function of x for different NC sizes. (b) Calculated spin-torque asymmetry λ and efficiency ϵ as functions of x; the red arrows mark the ϵ of NiFe and Co calculated from Ref. [30].

The spin-torque efficiency ϵ, and the spin-torque asymmetry λ are critical parameters to evaluate the energy efficiency of STT devices. A few studies [43,44] have attempted to extract these values experimentally with rather large uncertainty due to the magnetization's deviation and impact from imperfections of the devices. In contrast, our approach relies on two different contradicting behaviors in the magnetic droplet nucleation boundary, and this can provide a more accurate method to obtain the intrinsic STT parameters, the spin-torque efficiency ϵ, and the spin-torque asymmetry λ. Compared with the extraction of ϵ alone by linear fitting of the Slonczewski critical current from a single device [18,43], the simultaneous extraction of both parameters from a set of devices with different NC sizes offers high accuracy and reduces random variation. The parameters ϵ and λ extracted from Figs. 3(f)–3(j) are plotted as functions of x in Fig. 4(b). The spin-torque efficiency ϵ is almost constant at around 0.35, while the spin-torque asymmetry λ gradually increases from 1.5 to 3.0 as x increases. Note that the extracted λ of NiFe here is close to previous reports, where λ is approximately 1.34 in Ref. [18] and ~ 1.2 in Ref. [45]. We emphasize here that this is a systematic study of both λ and ϵ in different materials, and only a few prior studies [18,43,45] have reported on ϵ of NiFe and Co.

IV. CONCLUSIONS

We show the controllability of the nucleation boundary of magnetic droplet solitons in STNOs with an orthogonal spin-valve structure, where the saturation magnetization $\mu_0 M_{s,p}$ of the fixed layer, $Co_x(NiFe)_{1-x}$, is tuned by cosputtering of Co and NiFe. As x increases, the nucleation boundary shifts monotonically towards the higher magnetic field, which is consistent with the increasing $\mu_0 M_{s,p}$. By analyzing the droplet nucleation boundary we simultaneously extract the spin-torque efficiency ϵ and the spin-torque asymmetry λ for $Co_x(NiFe)_{1-x}$ thin films with high accuracy. While ϵ is largely independent on composition, λ shows a twofold increase from 1.5 to 3 with increasing Co content. Our results demonstrate the utility of the droplet nucleation boundary as a tool to accurately determine λ and ϵ of different materials.

ACKNOWLEDGMENTS

[1] M. A. Hoefer, T. J. Silva, and M. W. Keller, Theory for a dissipative droplet soliton excited by a spin torque nanocontact, Phys. Rev. B **82**, 054432 (2010).

[2] S. M. Mohseni, S. R. Sani, J. Persson, T. N. Anh Nguyen, S. Chung, Ye. Pogoryelov, P. K. Muduli, E. Iacocca, A. Eklund, R. K. Dumas, S. Bonetti, A. Deac, M. A. Hoefer, and J. Åkerman, Spin torque-generated magnetic droplet solitons, Science **339**, 1295 (2013).

[3] B. A. Ivanov and A. M. Kosevich, Bound states of a large number of magnons in a ferromagnet with a single-ion anisotropy, Zh. Ursp. Teor. Fiz. **72**, 2000 (1977).

[4] T. Chen, R. K. Dumas, A. Eklund, P. K. Muduli, A. Houshang, A. A. Awad, P. Dürrenfeld, B. G. Malm, A. Rusu, and J. Åkerman, Spin-torque and spin-Hall nano-oscillators, Proc. IEEE **104**, 1919 (2016).

[5] S. M. Mohseni, S. R. Sani, J. Persson, T. N. Anh Nguyen, S. Chung, Ye. Pogoryelov, and J. Åkerman, High frequency operation of a spin-torque oscillator at low field, Phys. Status Solidi - PRL **5**, 432 (2011).

[6] W. H. Rippard, A. M. Deac, M. R. Pufall, J. M. Shaw, M. W. Keller, S. E. Russek, G. E. W. Bauer, and C. Serpico, Spin-transfer dynamics in spin valves with out-of-plane magnetized CoNi free layers, Phys. Rev. B **81**, 014426 (2010).

[7] M. A. Hoefer, M. Sommacal, and T. J. Silva, Propagation and control of nanoscale magnetic-droplet solitons, Phys. Rev. B **85**, 214433 (2012).

[8] L. D. Bookman and M. A. Hoefer, Analytical theory of modulated magnetic solitons, Phys. Rev. B **88**, 184401 (2013).

[9] D. Xiao, V. Tiberkevich, Y. H. Liu, Y. W. Liu, S. M. Mohseni, S. Chung, M. Ahlberg, A. N. Slavin, J. Åkerman, and Y. Zhou, Parametric autoexcitation of magnetic droplet soliton perimeter modes, Phys. Rev. B **95**, 024106 (2017).

[10] S. Okamoto, N. Kikuchi, M. Furuta, O. Kitakami, and T. Shimatsu, Microwave assisted magnetic recording technologies and related physics, J. Phys. D: Appl. Phys. **48**, 353001 (2015).

[11] S. Bosu, H. Sepehri-Amin, Y. Sakuraba, S. Kasai, M. Hayashi, and K. Hono, High frequency out-of-plane oscillation with large cone angle in mag-flip spin torque oscillators for microwave assisted magnetic recording, Appl. Phys. Lett. **110**, 142403 (2017).

[12] M. D. Maiden, L. D. Bookman, and M. A. Hoefer, Attraction, merger, reflection, and annihilation in magnetic droplet soliton scattering, Phys. Rev. B **89**, 180409 (2014).

[13] V. Puliafito, G. Siracusano, B. Azzerboni, and G. Finocchio, Self-modulated soliton modes excited in a nanocontact spin-torque oscillator, IEEE Magn. Lett. **5**, 3000104 (2014).

[14] D. Xiao, Y. Liu, Y. Zhou, S. M. Mohseni, S. Chung, and J. Åkerman, Merging droplets in double nanocontact spin torque oscillators, Phys. Rev. B **93**, 094431 (2016).

[15] C. Wang, D. Xiao, Y. Zhou, J. Åkerman, and Y. Liu, Phase-locking of multiple magnetic droplets by a microwave magnetic field, AIP Adv. **7**, 056019 (2017).

[16] C. Wang, D. Xiao, and Y. Liu, Merging magnetic droplets by a magnetic field pulse, AIP Adv. **8,** 056021 (2018).

[17] M. Mohseni and M. Mohseni, Designing magnetic droplet soliton nucleation employing spin polarizer, Nanotechnology **29,** 155402 (2018).

[18] F. Macià, D. Backes, and A. D. Kent, Stable magnetic droplet solitons in spin transfer nanocontacts, Nat. Nanotechnol. **9,** 992 (2014).

[19] E. Iacocca, R. K. Dumas, L. Bookman, M. Mohseni, S. Chung, M. A. Hoefer, and J. Åkerman, Confined Dissipative Droplet Solitons in Spin-Valve Nanowires with Perpendicular Magnetic Anisotropy, Phys. Rev. Lett. **112,** 0477201 (2014).

[20] S. Chung, S. M. Mohseni, S. R. Sani, E. Iacocca, R. K. Dumas, T. N. Anh Nguyen, Ye. Pogoryelov, P. K. Muduli, A. Eklund, M. A. Hoefer, and J. Åkerman, Spin transfer torque generated magnetic droplet solitons (invited), J. Appl. Phys. **115,** 172612 (2014).

[21] S. Chung, S. M. Mohseni, A. Eklund, P. Dürrenfeld, M. Ranjbar, S. R. Sani, T. N. Anh Nguyen, R. K. Dumas, and J. Åkerman, Magnetic droplet solitons in orthogonal spin valves, Low Temp. Phys. **41,** 833 (2015).

[22] S. Lendínez, N. Statuto, D. Backes, A. D. Kent, and F. Macià, Observation of droplet soliton drift resonances in a spin-transfer-torque nanocontact to a ferromagnetic thin film, Phys. Rev. B **92,** 174426 (2015).

[23] D. Backes, F. Macià, S. Bonetti, R. Kukreja, H. Ohldag, and A. D. Kent, Direct Observation of a Localized Magnetic Soliton in a Spin-Transfer Nanocontact, Phys. Rev. Lett. **115,** 127205 (2015).

[24] M. Carpentieri, R. Tomasello, R. Zivieri, and G. Finocchio, Topological, non-topological and instanton droplets driven by spin-transfer torque in materials with perpendicular magnetic anisotropy and Dzyaloshinskii-Moriya interaction, Sci. Rep. **5,** 16184 (2015).

[25] S. Chung, A. Eklund, E. Iacocca, S. M. Mohseni, S. R. Sani, L. Bookman, M. A. Hoefer, R. K. Dumas, and J. Åkerman, Magnetic droplet nucleation boundary in orthogonal spin-torque nano-oscillators, Nat. Commun. **7,** 11209 (2016).

[26] S. Lendínez, J. Hang, D. Backes, A. D. Kent, and F. Macià, Effect of Temperature on Spin-Transfer Torque Induced Magnetic Solitons, Phys. Rev. Appl. **7,** 054027 (2017).

[27] B. Divinskiy, S. Urazhdin, V. E. Demidov, A. Kozhanov, A. P. Nosov, A. B. Rinkevich, and S. O. Demokritov, Magnetic droplet solitons generated by pure spin currents, Phys. Rev. B **96,** 224419 (2017).

[28] J. Hang, C. Hahn, N. Statuto, F. Macià, and A. D. Kent, Generation and annihilation time of magnetic droplet solitons, Sci. Rep. **8,** 6847 (2018).

[29] S. Jiang, S. R. Etesami, S. Chung, Q. T. Le, A. Houshang, and J. Åkerman, Impact of the oersted field on droplet nucleation boundaries, IEEE Magn. Lett. **9,** 3104304 (2018).

[30] W. H. Rippard, M. R. Pufall, and T. J. Silva, Quantitative studies of spin-momentum-transfer-induced excitations in Co/Cu multilayer films using point-contact spectroscopy, Appl. Phys. Lett. **82,** 1260 (2003).

[31] L. Berger, Emission of spin waves by a magnetic multilayer traversed by a current, Phys. Rev. B **54,** 9353 (1996).

[32] J. C. Slonczewski, Current-driven excitation of magnetic multilayers, J. Magn. Magn. Mater. **159,** L1 (1996).

[33] J. C. Slonczewski, Excitation of spin waves by an electric current, J. Magn. Magn. Mater. **195,** 261 (1999).

[34] J. C. Slonczewski, Currents and torques in metallic magnetic multilayers, J. Magn. Magn. Mater. **247,** 324 (2002).

[35] C. Kittel, On the gyromagnetic ratio and spectroscopic splitting factor of ferromagnetic substances, Phys. Rev. **76,** 743 (1949).

[36] M. R. Pufall, W. H. Rippard, M. L. Schneider, and S. E. Russek, Low-field current-hysteretic oscillations in spin-transfer nanocontacts, Phys. Rev. B **75,** 140404 (2007).

[37] S. Bonetti, V. Tiberkevich, G. Consolo, G. Finocchio, P. Muduli, F. Mancoff, A. Slavin, and J. Åkerman, Experimental Evidence of Self-Localized and Propagating Spin Wave Modes in Obliquely Magnetized Current-Driven Nanocontacts, Phys. Rev. Lett. **105,** 217204 (2010).

[38] V. E. Demidov, S. Urazhdin, and S. O. Demokritov, Direct observation and mapping of spin waves emitted by spin-torque nano-oscillators, Nat. Mater. **9,** 984 (2010).

[39] R. K. Dumas, E. Iacocca, S. Bonetti, S. R. Sani, S. M. Mohseni, A. Eklund, J. Persson, O. Heinonen, and J. Åkerman, Spin-Wave-Mode Coexistence on the Nanoscale: A Consequence of the Oersted-Field-Induced Asymmetric Energy Landscape, Phys. Rev. Lett. **110,** 257202 (2013).

[40] A. Hamadeh, N. Locatelli, V. V. Naletov, R. Lebrun, G. DeLoubens, J. Grollier, O. Klein, and V. Cros, Origin of Spectral Purity and Tuning Sensitivity in a Spin Transfer Vortex Nano-Oscillator, Phys. Rev. Lett. **112,** 257201 (2014).

[41] A. Houshang, E. Iacocca, P. Dürrenfeld, S. R. Sani, J. Åkerman, and R. K. Dumas, Spin-wave-beam driven synchronization of nanocontact spin-torque oscillators, Nat. Nanotechnol. **11,** 280 (2015).

[42] P. Wills, E. Iacocca, and M. A. Hoefer, Deterministic drift instability and stochastic thermal perturbations of magnetic dissipative droplet solitons, Phys. Rev. B **93,** 144408 (2016).

[43] M. R. Pufall, W. H. Rippard, and T. J. Silva, Materials dependence of the spin-momentum transfer efficiency and critical current in ferromagnetic metal/Cu multilayers, Appl. Phys. Lett. **83,** 323 (2003).

[44] D. Ralph and M. Stiles, Spin transfer torques, J. Magn. Magn. Mater. **320,** 1190 (2008).

[45] P. M. Braganca, I. N. Krivorotov, O. Ozatay, A. G. F. Garcia, N. C. Emley, J. C. Sankey, D. C. Ralph, and R. A. Buhrman, Reducing the critical current for short-pulse spin-transfer switching of nanomagnets, Appl. Phys. Lett. **87,** 112507 (2005).